PROCEEDINGS OF SCIENCE

Light Quark Spectroscopy at BESIII

Fang Liu[*†]
Institute of High Energy Physics, Chinese Academy of Sciences, Beijing, China
E-mail: liufang@mail.ihep.ac.cn

The BESIII experiment at the Beijing Electron and Positron Collider is successfully operating since 2008 and has collected large data samples in the tau-mass region, including the world's largest data samples of J/ψ, $\psi(3686)$, $\psi(3770)$ and $\psi(4040)$ decays. In particular J/ψ and $\psi(3686)$ decays provides a rich and clean environment to study light quark spectroscopy. Many latest experimental searches on the $p\bar{p}$ mass threshold enhancement and $X(1835)$ have been performed by BESIII Collaboration with a high statistical events and provides valuable information that helps to clarify the nature of the states around 1.8 GeV. A Partial Wave Analysis (PWA) of the system $\pi^0\pi^0$ is shown with a focus on the parametrization of the the $\pi\pi$ scattering amplitude. A PWA of the decay $J/\psi \to \gamma\phi\phi$ shows that the intermediate states in the $\phi\phi$ invariant mass are dominantly 0^{-+} states, in which the $\eta(2225)$ is confirmed. In this presentation recent results of the light quark spectroscopy will be highlighted.

Flavor Physics and CP Violation,
6-9 June 2016
Caltech, Pasadena CA, USA

[*]Speaker.
[†]on behalf of BESIII Collaboration

PoS(FPCP2016)035

1. Introduction

Glueballs and other resonances with large gluonic components are predicted as bound states by QCD. The lightest (scalar) glueballs is estimated to have a mass in the range from 1 to 2 GeV/c^2; pseudoscalar and tensor glueballs are expected at higher masses. Radiative decays of the charmonium provide a glueon rich environment and are therefore regarded as one of the most promising hunting grounds for glueballs and hybrids.

BESIII (Beijing Spectrometer) is a general purpose 4π detector at the upgraded BEPCII (Beijing Electron and Positron Collider) that operated in the $\tau-$ charm threshold energy region [1]. Since 2009, it has collected the world's largest samples of J/ψ, $\psi(3686)$, $\psi(3770)$ and $\psi(4040)$ decays. More recently, data were taken in the energy region above 4 GeV, where energies up to about 4.6 GeV are accessible. These data are being used to make a variety of interesting and unique studies of light hadron spectroscopy, charmonium spectroscopy, high statistic measurements of charmonium decays and D meson decays.

2. Light Quark Spectroscopy

2.1 $p\bar{p}$ Mass threshold enhancement and $X(1835)$

An anomalously strong $p\bar{p}$ mass threshold enhancement was first observed by the BESII experiment in the radiative decay process $J/\psi \to \gamma p\bar{p}$ [2] and was recently confirmed by the BESIII and CLEO-c [3] experiments. Curiously, no apparent corresponding structures were seen in near-threshold $p\bar{p}$ cross section measurements, in B-meson decays [4], in radiative ψ' or $\Upsilon \to \gamma p\bar{p}$ decays [5]. These non-observations disfavor the mass-threshold enhancement attribution to the effects of $p\bar{p}$ final state interactions (FSI) [6, 7, 8].

A number of theoretical speculations have been proposed to interpret the nature of this structure [6, 7, 8, 9, 10, 11, 12]. Among them, one intriguing suggestion is that it is due to a $p\bar{p}$ bound state, sometimes called baryonium [12], an object with a long history and the subject of many experimental searches [13]. The observation of the $p\bar{p}$ mass threshold enhancement also stimulated many experimental analyses on BESIII experiment.

The Partial Wave Analysis (PWA) of $J/\psi \to \gamma p\bar{p}$ and $\psi' \to \gamma p\bar{p}$ decays are performed using 225 Million J/ψ and 106 Million ψ' events [14]. In J/ψ radiative decays, the events with $M_{p\bar{p}} < 2.2\text{GeV}/c^2$ are composed of significant $p\bar{p}$ mass threshold enhancement $X(p\bar{p})$, $f_2(1920)$ and $f_0(2100)$ and non-resonant 0^{++} phase space, as shown in PWA results of Fig. 1. The near-threshold enhancement $X(p\bar{p})$ is determined to be a 0^{-+} state. With the inclusion of Julich-FSI effects, the mass, width and product branching fraction (BR) for the $X(p\bar{p})$ are measured to be: $M = 1832^{+19}_{-5}\ (\text{stat})^{+18}_{-17}\ (\text{syst}) \pm 19\ (\text{model})\ \text{MeV}/c^2$, $\Gamma = 13 \pm 39\ (\text{stat})^{+10}_{-13}\ (\text{syst}) \pm 4\ (\text{model})\ \text{MeV}/c^2$ (a total width of $\Gamma < 76\ \text{MeV}/c^2$ at the 90% C.L) and $\mathscr{B}(J/\psi \to \gamma X) \times \mathscr{B}(X \to p\bar{p}) = (9.0^{+0.4}_{-1.1}(\text{stat})\ ^{+1.5}_{-5.0}(\text{syst}) \pm 2.3(\text{model})) \times 10^{-5}$, respectively. The product BR for $X(p\bar{p})$ in ψ' decay is first measured to be $\mathscr{B}(\psi' \to \gamma X) \times \mathscr{B}(X \to p\bar{p}) = (4.57 \pm 0.36\ (\text{stat})^{+1.23}_{-4.07}\ (\text{syst}) \pm 1.28\ (\text{model})) \times 10^{-6}$ and the ratio of product branching fractions for the $X(p\bar{p})$ between J/ψ and ψ' radiative decays is $R = (5.08^{+0.71}_{-0.45}\ (\text{stat})^{+0.67}_{-3.58}\ (\text{syst}) \pm 0.12\ (\text{model}))\%$.

Study of the hadronic decays $J/\psi \to \omega p\bar{p}$ and $\phi p\bar{p}$ may also shed further light on the nature of $X(p\bar{p})$. The decay $J/\psi \to \omega p\bar{p}$ has been studied [15], using 225.3×10^6 J/ψ events accumulated at BESIII in 2009. No significant enhancement $X(p\bar{p})$ near the $p\bar{p}$ invariant-mass threshold is observed as shown in Fig. 2. The upper limit of the branching fraction $\mathscr{B}(J/\psi \to \omega X(p\bar{p}) \to \omega p\bar{p})$ is determined to be 3.9×10^{-6} at the 95% confidence level, which is suppressed with one order of magnitude comparing to the branching fraction of $J/\psi \to \gamma X(p\bar{p}) \to \gamma p\bar{p}$. Another hadronic decay $J/\psi \to p\bar{p}\phi$ is studied [16] via two decay modes, $\phi \to K_S K_L$ and $\phi \to K^+K^-$, using a data sample of 1.31×10^9 J/ψ events accumulated with the BESIII detector in 2009 and 2012. No evident enhancement $X(p\bar{p})$ near the $p\bar{p}$ mass threshold, is observed as shown in Fig. 3, and the upper limit on the branching fraction of $J/\psi \to X(p\bar{p})\phi \to p\bar{p}\phi$ is determined to be $\mathscr{B}(J/\psi \to X(p\bar{p})\phi \to p\bar{p}\phi) < 2.1 \times 10^{-7}$ at the 90% confidence level, which is much suppressed with two order of magnitude comparing to that of $J/\psi \to \gamma X(p\bar{p}) \to \gamma p\bar{p}$.

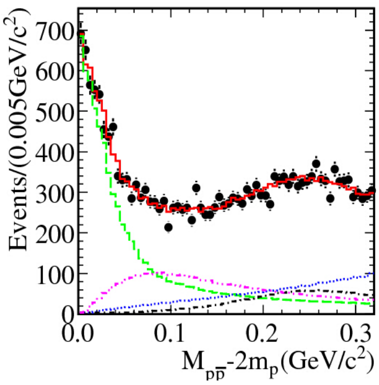

Figure 1: Comparisons of the $p\bar{p}$ invariant mass between data and PWA fit projection. The black dots with error bars are data, the solid histograms show the PWA total projection, and the dashed, dotted , dash-dotted and dash-dot-dotted lines show the contributions of the $X(p\bar{p})$, 0^{++} phase space, $f_0(2100)$ and $f_2(1910)$, respectively.

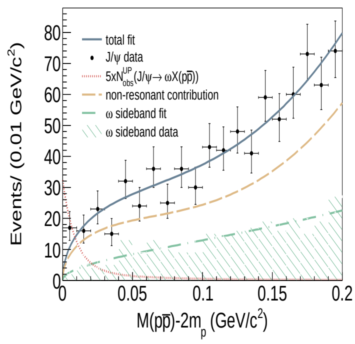

Figure 2: Near-threshold $p\bar{p}$ invariant-mass spectrum. The signal $J/\psi \to \omega X(p\bar{p}) \to \omega p\bar{p}$ is described by an acceptance-weighted Breit-Wigner function, and and signal yield is consistent with zero. The dotted line is the shape of the signal which is normalized to five times the estimated upper limit. The hatched area is from the sideband region.

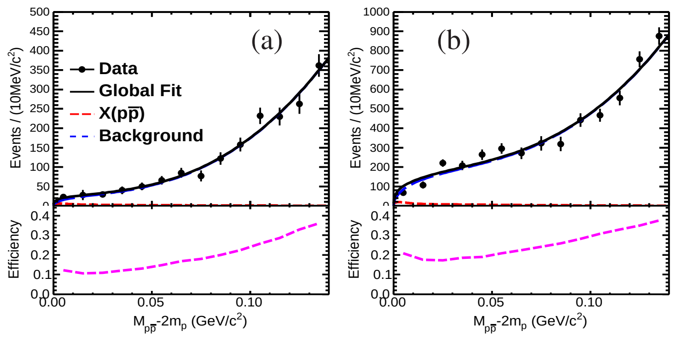

Figure 3: Distributions of $M_{p\bar{p}} - 2m_p$ and the fit results corresponding to the upper limit on the branching fraction at the 90% C.L., the dashed line at the bottom is the efficiency as a function of the $p\bar{p}$ mass, (a) for $\phi \to K^0_S K^0_L$, (b) for $\phi \to K^+K^-$.

The observation of the $p\bar{p}$ mass threshold enhancement also stimulated an experimental analysis of $J/\psi \to \gamma\pi^+\pi^-\eta'$ decays, in which a $\pi^+\pi^-\eta'$ resonance, the $X(1835)$, was first observed by the BESII experiment [17]. A high statistics data sample collected with BESIII in 2009 provides an opportunity to confirm the existence of the $X(1835)$ and look for possible related states that decay to $\pi^+\pi^-\eta'$. The decay $J/\psi \to \gamma\pi^+\pi^-\eta'$ is studied [18] combining two η' decay modes: $\eta' \to \pi^+\pi^-\eta$ and $\eta' \to \gamma\rho^0$. The $X(1835)$ in the $\eta'\pi^+\pi^-$ invariant mass as shown in Fig. 4 is confirmed with a statistical significance that is larger than 20σ. In addition, in the $\pi^+\pi^-\eta'$ invariant mass spectrum, the $X(2120)$ and the $X(2370)$, are observed with statistical significances larger than 7.2σ and 6.4σ, respectively. For the $X(1835)$, the angular distribution of the radiative photon is consistent with expectations for a pseudoscalar, but other spin-parity assignment is not excluded. Then systematic studies of $X(1835)$ are ongoing at BESIII to understand its nature, measurement of its J^{PC} and search for new decays modes is very crucial.

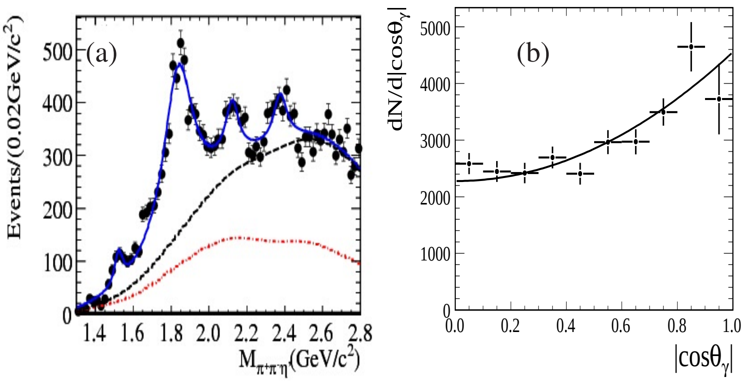

Figure 4: The $\pi^+\pi^-\eta'$ mass spectrum fitting with four resonances (a) and acceptance-corrected $|\cos\theta_\gamma|$ distribution of the $X(1835)$ (b). For (a), the dash-dot line is contributions of non-η' events and the $\pi^0\pi^+\pi^-\eta'$ background for two η' decay modes and the dash line is contributions of the total background and non-resonant $\pi^+\pi^-\eta'$ process.

We study a new decay mode $J/\psi \to \gamma K^0_S K^0_S \eta$ [19] using data sample of 1.31×10^9 J/ψ events collected with the BESIII detector. Figure 5 (a) shows the scatter plot of the invariant mass of $K^0_S K^0_S$ versus $K^0_S K^0_S \eta$, indicating the structure around 1.85 GeV$/c^2$ is strong correlated with $f_0(980)$. A partial wave analysis of $J/\psi \to \gamma K^0_S K^0_S \eta$ has been performed in the mass range $M_{K^0_S K^0_S \eta} < 2.8$ GeV$/c^2$ after requiring $M_{K^0_S K^0_S} < 1.1$ GeV$/c^2$. Figures 5 (b) and (c) are the invariant mass distribution of $K^0_S K^0_S \eta$ and $K^0_S K^0_S$. Overlaid on the data are the PWA fit projections, as well as the individual contributions from each component. The PWA fit requires a contribution from $X(1835) \to \gamma K^0_S K^0_S \eta$ with a statistical significance larger than 12.9σ, whether $X(1835) \to \gamma K^0_S K^0_S \eta$ is dominated by $f_0(980)$ production. The spin parity of the $X(1835)$ is determined to be 0^{-+}. The mass and width of the $X(1835)$ are measured to be $1844 \pm 9(\text{stat})^{+16}_{-25}(\text{syst})$ MeV and $192^{+20}_{-17}(\text{stat})^{+62}_{-43}(\text{syst})$ MeV, respectively. The corresponding product branching fraction is measured to be $(3.31^{+0.33}_{-0.30}(\text{stat})^{+1.96}_{-1.29}(\text{syst})) \times 10^{-5}$. The mass and width of the $X(1835)$ are consistent with the values obtained from the decay $J/\psi \to \gamma\pi^+\pi^-\eta'$ [18]. These results are all first-times measurements and provide important information to further understand the nature of the $X(1835)$. Another 0^{-+} state, the $X(1560)$, is also observed in data with a statistical significance larger than 8.9σ. The mass and width of the $X(1560)$ are consistent with those of the $\eta(1405)$ and $\eta(1475)$ as given in Ref. [20] within 2.0σ and 1.4σ, respectively.

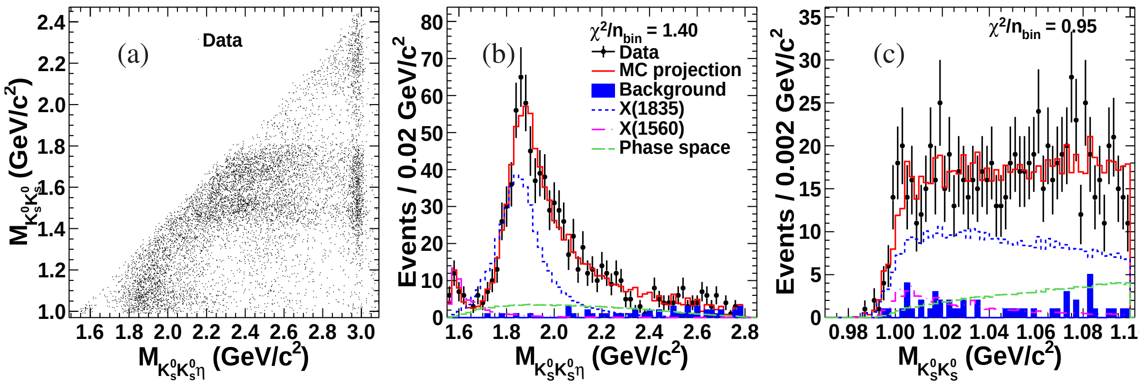

Figure 5: The scatter plot of $M_{K_S^0K_S^0}$ versus $M_{K_S^0K_S^0\eta}$; Comparisons between data and PWA fit projections. (b), and (c) are the invariant mass distributions of $M_{K_S^0K_S^0\eta}$ and $M_{K_S^0K_S^0}$. The dots with error bars are data, the solid histograms are the PWA total projections, the shaded histograms are the non-η backgrounds estimated by the η sideband, and the short-dashed, dash-dotted, and long-dashed histograms show the contributions of $X(1835)$, $X(1560)$, and the non-resonant component, respectively.

The above experimental results stimulate many various theoretical interpretations on the nature of the $X(1835)$ and $X(p\bar{p})$ [9, 10, 11, 21, 22], a particularly intriguing one suggests that the two structures originate from a $p\bar{p}$ bound state [23, 24, 25, 26, 27]. If the $X(1835)$ is really a $p\bar{p}$ bound state, it should have a strong coupling to 0^- $p\bar{p}$ systems, in which case the line shape of $X(1835)$ at the $p\bar{p}$ mass threshold would be affected by the opening of the $X(1835) \to p\bar{p}$ decay mode. A study of the $\eta'\pi^+\pi^-$ line shape of $X(1835)$ with high statistical precision therefore provides valuable information that helps clarify the nature of the $X(1835)$ and $X(p\bar{p})$. We use a total sample of 1.09×10^9 J/ψ decay events [28] accumulated by the BESIII experiment in 2012, and report the observation of a significant abrupt change in slope of the $X(1835) \to \eta'\pi^+\pi^-$ line shape at the $p\bar{p}$ mass threshold in a larger sample of $J/\psi \to \gamma\eta'\pi^+\pi^-$ events [29] collected in the BESIII detector at the BEPCII e^+e^- storage ring. The η' is also reconstructed in its two major decay modes: $\eta' \to \gamma\pi^+\pi^-$ and $\eta' \to \eta\pi^+\pi^-$ ($\eta \to \gamma\gamma$). Figure 6 shows the $\eta'\pi^+\pi^-$ invariant mass spectra after all selection criteria, where peaks corresponding to the $X(1835)$, $X(2120)$, $X(2370)$, η_c, and a structure near 2.6 GeV that has not been seen before are evident for both η' decays. Thanks to the high statistical precision, an abrupt change in slope of the $X(1835)$ line shape at the $p\bar{p}$ mass threshold is evident in both event samples.

We perform simultaneous fits to the $\eta'\pi^+\pi^-$ invariant mass distributions between 1.3 GeV and 2.25 GeV for both selected event samples, and the significant distortion of the $\eta'\pi^+\pi^-$ line shape near the $p\bar{p}$ mass threshold cannot be accommodated by an ordinary Breit-Wigner resonance function as shown in Fig. 7 (a). Two typical models for such a line shape are used to fit the data. The first model assumes the state around 1.85 GeV couples with $p\bar{p}$ and the distortion reflects the opening of the $p\bar{p}$ decay channel. The fit result for this model, as shown in Fig. 7 (b), yields a strong coupling between the broad structure and the $p\bar{p}$ of $\frac{g^2_{p\bar{p}}}{g^2_0} = 2.31 \pm 0.37^{+0.83}_{-0.60}$, with a statistical significance larger than 7σ for being non-zero. The pole nearest to the $p\bar{p}$ mass threshold of this state is located at $M_{\rm pole} = 1909.5 \pm 15.9(\rm stat)^{+9.4}_{-27.5}(\rm syst)$ MeV and $\Gamma_{\rm pole} = 273.5 \pm 21.4(\rm stat)^{+6.1}_{-64.0}(\rm syst)$ MeV. The second model assumes the distortion reflects interference between the $X(1835)$ and an-

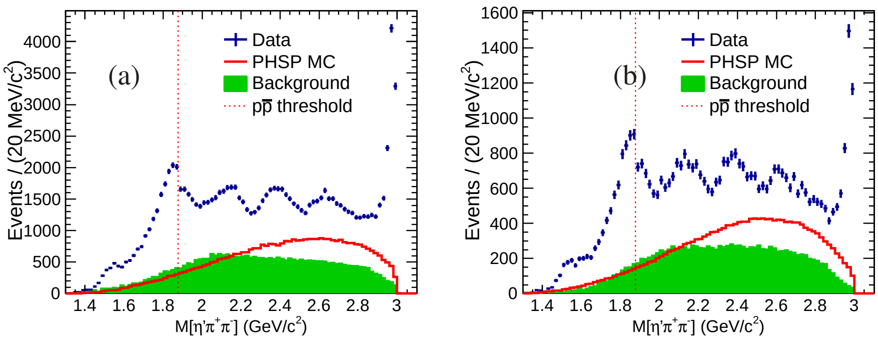

Figure 6: The $\eta'\pi^+\pi^-$ invariant mass spectra with the $\eta' \to \gamma\pi^+\pi^-$ channel (a) and $\eta' \to \eta(\to \gamma\gamma)\pi^+\pi^-$ channel (b). In both plots, the dots with error bars are data, the shaded histograms are the background, the solid histograms are phase space (PHSP) MC events of $J/\psi \to \gamma\eta'\pi^+\pi^-$ (arbitrary normalization), the dotted vertical line shows the position of $p\bar{p}$ mass threshold.

other resonance with mass close to the $p\bar{p}$ mass threshold. A fit with this model uses a coherent sum of two interfering Breit-Wigner amplitudes to describe the $\eta'\pi^+\pi^-$ mass spectrum around 1.85 GeV. This fit, as shown in Fig. 7 (c), yields a narrow resonance below the $p\bar{p}$ mass threshold with $M = 1870.2 \pm 2.2(\text{stat})^{+2.3}_{-0.7}(\text{syst})$ MeV and $\Gamma = 13.0 \pm 6.1(\text{stat})^{+2.1}_{-3.8}(\text{syst})$ MeV, with a statistical significance larger than 7σ. With current data, both models fit the data well with fit qualities, and both suggest the existence of a state, either a broad state with strong couplings to $p\bar{p}$, or a narrow state just below the $p\bar{p}$ mass threshold. For the broad state above the $p\bar{p}$ mass threshold, its strong couplings to $p\bar{p}$ suggests the existence of a $p\bar{p}$ molecule-like state. For the narrow state just below $p\bar{p}$ mass threshold, its very narrow width suggests that it be an unconventional meson, most likely a $p\bar{p}$ bound state. So both fits support the existence of a $p\bar{p}$ molecule-like or bound state. With current statistics, more sophisticated models such as a mixture of above two models cannot be ruled out. In order to elucidate further the nature of the states around 1.85 GeV, more data are needed to further study $J/\psi \to \gamma\eta'\pi^+\pi^-$ process. Also, line shapes for other decay modes should be studied near the $p\bar{p}$ mass threshold, including further studies of $J/\psi \to \gamma p\bar{p}$ and $J/\psi \to \gamma K^0_S K^0_S \eta$.

2.2 Amplitude analysis of the $\pi^0\pi^0$ system produced in radiative J/ψ decay

A mass independent amplitude analysis of the $\pi^0\pi^0$ system in radiative decays is performed [30]. This analysis uses the world's largest sample of its type, collected with the BESIII detector, to extract a piecewise function that describes the scalar and tensor $\pi\pi$ amplitudes in this decay. While the analysis strategy employed to obtain results has complications, namely ambiguous solutions, a large number of parameters, and potential bias in subsequent analysis from non-Gaussian effects, its minimizes systematic bias arising from assumptions about $\pi\pi$ dynamics, and consequently, permits the developments of dynamical models or parameterizations for the data.

The intensities and phase differences for the amplitudes in the fit are presented as a function of $M_{\pi^0\pi^0}$ in Ref. [30]. Additionally, in order to facilitate the development of models, the intensities and phases of each bin of $M_{\pi^0\pi^0}$ are given in supplemental materials. These results may be combined with those of similar reactions for a more comprehensive study of the light scalar meson spectrum.

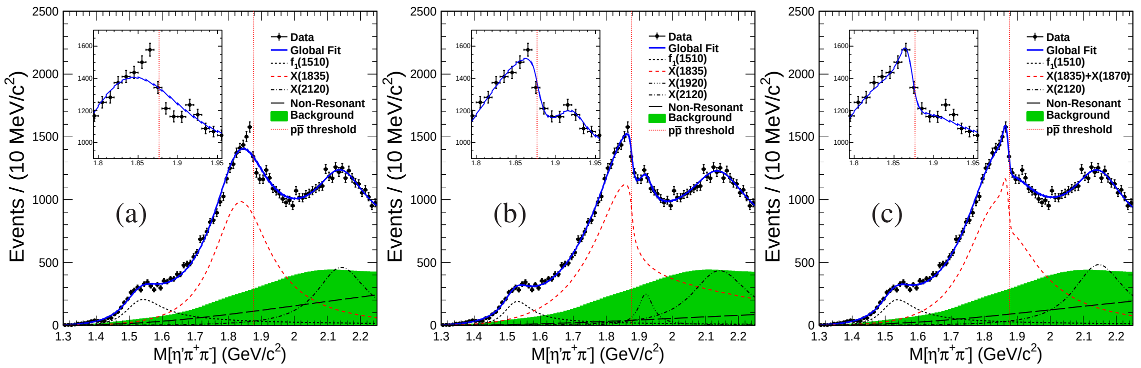

Figure 7: Fit results with simple Breit-Wigner formulae (a), using Flatté formula (b) and using a coherent sum of two Breit-Wigner amplitudes (c), respectively. The dashed dotted vertical line shows the position of $p\bar{p}$ mass threshold, the dots with error bars are data, the solid curves are total fit results, the short-dashed curves the $f_1(1510)$, the dash-dot curves the $X(2120)$, and the long-dashed curves are the non-resonant $\eta'\pi^+\pi^-$ fit results; the shaded histograms are background events. The dashed curves are the $X(1835)$, the state around 1.85 GeV and the sum of $X(1835)$ and $X(1870)$ for (a) (b) and (c) respectively. The inset shows the data and the global fit between 1.8 GeV and 1.95 GeV.

Finally, the branching fraction of radiative J/ψ decays to $\pi^0\pi^0$ is measured to be $(1.15\pm0.05)\times 10^{-3}$, where the error is systematic only and the statistical error is negligible. This is the first measurement of this branching fraction.

2.3 Partial Wave Analysis of $J/\psi \to \gamma\phi\phi$

The low lying pseudoscalar glueball is predicted to be around $2.3-2.6$ GeV$/c^2$ by Lattice QCD [31]. Aside from the $\eta(2225)$, very little is known in the pseudoscalar sector above 2 GeV$/c^2$. A partial wave analysis of the decay of $J/\psi \to \gamma\phi\phi$, as shown in Fig. 8, is performed [32] in order to study the intermediate states. The most remarkable feature of the PWA results is that 0^{-+} states are dominant. The existence of the $\eta(2225)$ is confirmed and two additional pseudoscalar states, $\eta(2100)$ with a mass of 230^{+64+77}_{-35-26} MeV$/c^2$ and a width $250^{+36+187}_{-30-164}$ MeV$/c^2$ and $X(2500)$ with a mass 2470^{+15+63}_{-19-23} MeV$/c^2$ and a width 230^{+64+53}_{-35-33} MeV$/c^2$, are obtained. The new experimental results are helpful for mapping out pseudoscalar excitations and search for a 0^{-+} glueball. The three tensors $f_2(2100)$, $f_2(2300)$ and $f_2(2340)$ observing $\pi^- p \to \phi\phi n$ [33] are also observed in $J/\psi \to \gamma\phi\phi$. Recently, the production rate of the pure gauge tensor glueball in J/ψ radiative decays has been predicted by Lattice QCD [34], which is compatible with the large production rate of the $f_2(2340)$ in $J/\psi \to \gamma\phi\phi$ and $J/\psi \to \gamma\eta\eta$ [35].

3. Summary

With the world's largest sample of J/ψ, $\psi(3686)$, $\psi(3770)$ and Y(4040). From e^+e^- production, the BESIII experiment made a significant contribution to the study of the light quark spectroscopy. BESIII will continue to run $6-8$ years. Complementary to other experiment, with various production mechanisms, BESIII will give more interesting results and continue shedding light on the nature of hadrons.

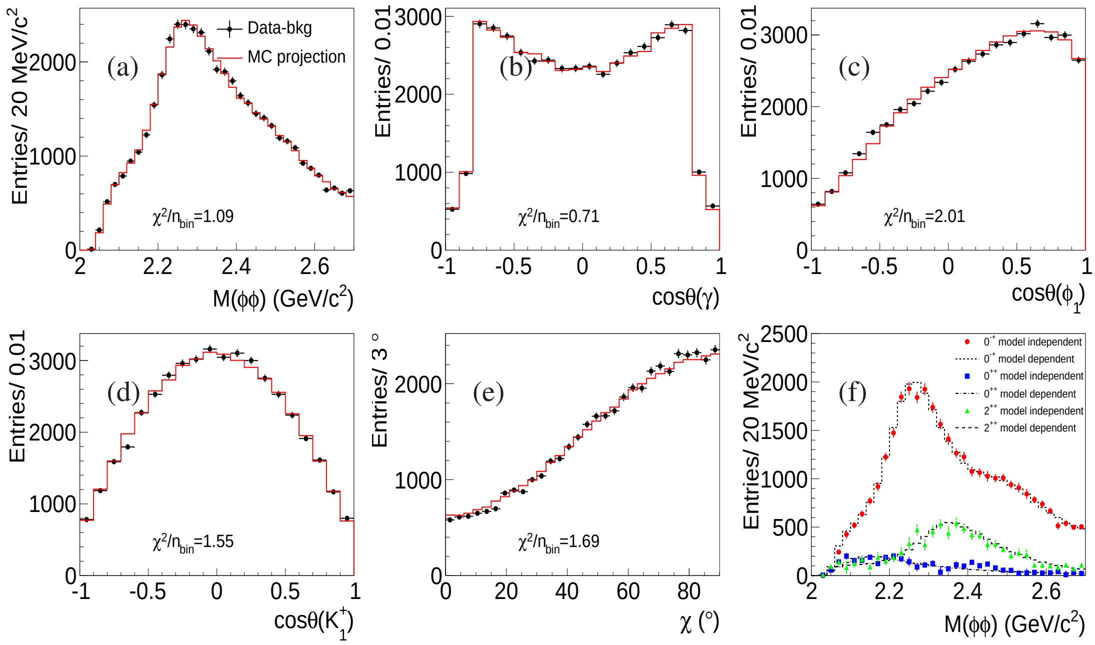

Figure 8: Superposition of data and the PWA fit projections for: (a) invariant mass distributions of $\phi\phi$; (b) $\cos\theta$ of γ in the J/ψ rest frame; (c) $\cos\theta$ of ϕ_1 in the X rest frame; (d) $\cos\theta$ of K^+ in the ϕ_1 rest frame; (e) the azimuthal angle between the normals to the two decay planes of ϕ in the X rest frame. Black dots with error bars are data with background events subtracted and the solid red lines are projections of the model-dependent fit. (f) Intensities of individual J^{PC} components. The red dots, blue boxes and green triangles with error bars are the intensities of $J^{PC} = 0^{-+}$, 0^{++} and 2^{++}, respectively, from the model-independent fit in each bin. The short-dashed, dash-dotted and long-dashed histograms show the coherent superpositions of the BW resonances with $J^{PC} = 0^{-+}$, 0^{++} and 2^{++}, respectively, from the model-dependent fit.

References

[1] M. Ablikim *et al.* (BESIII Collaboration), Nucl. Instrum. Meth. A **614**, 345 (2010).

[2] J.Z. Bai *et al.* (BES Collaboration), Phys. Rev. Lett. **91**, 022001 (2003).

[3] M. Ablikim *et al.* (BESIII Collaboration), Chin.Phys. **C34**, 421 (2010); J. P. Alexander *et al.* (CLEO Collaboration), Phys. Rev. **D 82**, 092002 (2010).

[4] S. Jin, Int. J. Mod. Phys. **A 20**, 5145 (2005); M.Z. Wang *et al.*, Phys. Rev. Lett. **92**, 131801 (2004).

[5] M. Ablikim *et al.* (BES Collaboration), Phys. Rev. Lett. **99**, 011802 (2007); S.B. Athar *et al.* (CLEO Collaboration), Phys. Rev. **D 73**, 032001 (2006).

[6] A. Sirbirtsen *et al.*, Phys. Rev. **D 71**, 054010 (2005).

[7] G. Y. Chen *et al.*, Phys. Lett. **B 692**, 136 (2010).

[8] B. S. Zou and H. C. Chiang, Phys. Rev. **D 69**, 034004 (2003).

[9] X. H. Liu *et al.*, Phys. Rev. **D 80**, 034032 (2009);

[10] N. Kochelev and D. P. Min, Phys. Lett. **B 633**, 283 (2006).

[11] T. Huang and S. L. Zhu, Phys. Rev. **D 73**, 014023 (2006).

[12] A. Datta and P. J. ODonnel, Phys. Lett. **B 567**, 273 (2003); M. L. Yan *et al.*, Phys. Rev. **D 72**, 034027 (2005); B. Loiseau *et al.*, Phys. Rev. **C 72**, 011001 (2005).

[13] E. Klempt *et al.*, Phys. Rep. **368**, 119 (2002).

[14] M. Ablikim *et al.* (BES Collaboration), Phys. Rev. Lett. **108**, 112003 (2012).

[15] M. Ablikim *et al.* (BES Collaboration), Phys. Rev. **D 87**, 112004 (2013).

[16] M. Ablikim *et al.* (BES Collaboration), Phys. Rev. **D 93**, 052010 (2016).

[17] M. Ablikim *et al.* (BES Collaboration), Phys. Rev. Lett. **95**, 262001 (2005).

[18] M. Ablikim *et al.* (BESIII Collaboration), Phys. Rev. Lett. **106**, 072002 (2011).

[19] M. Ablikim *et al.* (BESIII Collaboration), Phys. Rev. Lett. **115**, 091803 (2015).

[20] K. A. Olive *et al.* (Particle Data Group), Chin. Phys. **C 38**, 090001(2014).

[21] G. Hao, C. F. Qiao and A. L. Zhang, Phys. Lett. **B 642**, 53 (2006).

[22] B. A. Li, Phys. Rev. **D 74**, 034019 (2006).

[23] J. P. Dedonder *et al.*, Phys. Rev. **C 80**, 045207 (2009).

[24] C. Liu, Eur. Phys. J. **C 53**, 413 (2008).

[25] Z. G. Wang and S. L. Wan, J. Phys. **34**, 505 (2007).

[26] S. L. Zhu and C. S. Gao, Commun. Theor. Phys. **46**, 291 (2006).

[27] G. J. Ding, R. G. Ping, and M. L. Yan, Eur. Phys. J. A **28**, 351 (2006).

[28] M. Ablikim *et al.* (BESIII Collaboration), Chin. Phys. C **36**, 915 (2012).

[29] M. Ablikim *et al.* (BESIII Collaboration), Phys. Rev. Lett. **117**, 042002 (2016).

[30] M. Ablikim *et al.* (BESIII Collaboration), Phys. Rev. **D 92**, 052003 (2015).

[31] C. Amsler and N. A. Tornqvist, Phys. Rev. **389**, 61 (2004); E. Klempt and A. Zaitsev, Phys. Rep. **454**, 1 (2007);

[32] M. Ablikim *et al.* (BESIII Collaboration), Phys. Rev. **D 93**, 112011 (2016).

[33] A. Etkin *et al.* Phys. Rev. Lett. **41**, 784 (1978); Phys. Lett. **B 165**, 217 (1985); Phys. Lett. **B 201**, 568 (1988).

[34] Y. Chen *et al.*, Phys. Rev. Lett. **111**, 091601 (2013).

[35] M. Ablikim *et al.* (BESIII Collaboration), Phys. Rev. **D 87**, 092009 (2013).